Chiral and racemic spin crossover polymorphs in a family of mononuclear Iron(II) compounds

Carlos Bartual-Murgui,[a] Lucía Piñeiro-López,[a] F. Javier Valverde-Muñoz,[a] M. Carmen Muñoz,[b] Maksym Seredyuk,[a,c] José Antonio Real*[a]*

[a]Institut de Ciència Molecular (ICMol), Departament de Química Inorgànica Universitat de València C/ Catedrático José Beltrán Martínez, 2, 46980 Paterna (Valencia), Spain.

[b]Departament de Física Aplicada Universitat Politècnica de València Camino de Vera s/n, 46022 Valencia, Spain.

[c]Taras Shevchenko National University, Department of Chemistry, Volodymyrska Str. 64, Kyiv 01601, Ukraine

ABSTRACT

Understanding the origin of cooperativity and the equilibrium temperature of transition ($T_{1/2}$) displayed by the spin-crossover (SCO) compounds as well as controlling these parameters are of paramount importance for future applications. For this task, the occurrence of polymorphism, presented by a number of SCO complexes, may provide deep insight into the influence of the supramolecular organization on the SCO behavior. In this context, herein we present a novel family of mononuclear octahedral Fe^{II} complexes with formula *cis*-[Fe(bqen)$(NCX)_2$] where bqen is the chelating tetradentate ligand N,N'-Bis(8-quinolyl)ethane-1,2-diamine and X = S or Se. Depending on the preparation method, these compounds crystallize either in the orthorhombic or the trigonal symmetry systems. While the orthorhombic phase is composed of a racemic mixture of mononuclear complexes (polymorph I), the trigonal phase contains only one of the two possible enantiomers (Λ or Δ) thereby generating a chiral crystal (polymorph II). The four derivatives undergo SCO behavior with well-differentiated $T_{1/2}$ occurring in the interval 90-233 K. On one hand, $T_{1/2}$ is about 110 K (polymorph I) and 87 K (polymorph II) higher for the selenocyanate derivatives than for their thiocyanate counterparts. These differences in $T_{1/2}$ are ascribed not only to the higher ligand field induced by the selenocyanate anion but also to a remarkably difference in the structural reorganization of the [FeN_6] coordination core upon SCO.

Likewise, the higher cooperativity observed for the thiocyanate derivatives seems to be related to their stronger intermolecular interactions within the crystal. On the other hand, $T_{1/2}$ is about 53 K (thiocyanate) and 29 K (selenocyanate) higher for the trigonal polymorph II than for the orthorhombic polymorph I. These differences, and the small changes observed in cooperativity, stem from the slightly different hetero- and homochiral crystal packing generated by the cis-$[Fe(bqen)(NCX)_2]$ molecules, which determines subtle adaptations in the intermolecular contacts and the Fe^{II} coordination core.

INTRODUCTION

The spin crossover (SCO) phenomenon is an outstanding example of molecular switching displayed by some coordination complexes containing transition metals with $3d^4$-$3d^7$ electronic configurations. Among them, octahedral SCO Fe^{II} ($3d^6$) complexes have been, largely, the most aimed and investigated systems. This is likely because the transition between the low spin (LS) ($S = 0$, $t_{2g}^6e_g^0$) and the high spin (HS) ($S = 2$, $t_{2g}^4e_g^2$) states is accompanied by measurable changes in the magnetic, electric and optical properties.[1]

Even if thermally-driven spin transition compounds have been traditionally the most studied and published systems, the spin state change can also be triggered by the modification of pressure,[2] a magnetic field,[3] light irradiation[4] or guest adsorption processes.[5] These switchable properties make these complexes excellent candidates for memories and sensor applications.[6]

At the macroscopic scale, the transmission efficiency of the spin-state change within the material is determined by its cooperativity. Hence, materials presenting low cooperativity (weak coupling between SCO centers) will display smooth SCO curves whereas those presenting high cooperativity (strong coupling between SCO centers) will exhibit abrupt spin transitions.[7] Thus, in principle, cooperative transitions are expected for extended polymeric systems (1-3D frameworks) in which the SCO metal ions are connected through rigid bonds, allowing an efficient propagation of the spin state change. However, it is well documented that in the case of discrete mononuclear complexes (0D systems), the lack of covalent connections between Fe^{II} centers does not mean, necessarily, a low degree of cooperativity. This is because the packing of the molecular complexes can be established on the basis of a strong and dense lattice of intermolecular forces (i.e. π···π, π···HC and / or hydrogen bonds) conferring high cooperative effects.[8]

The transition temperature ($T_{1/2}$), defined as the temperature of equilibrium at which the molar fraction of the HS centers is equal to that of the LS centers ($\gamma_{HS} = \gamma_{LS} = 0.5$) is, together with the cooperativity, the other main parameter defining the SCO behavior. As it was mentioned before, the latter depends on how efficient the connectivity between the Fe^{II} centers is, whereas the former is rather related to the octahedral environment of the metal center. Indeed, weak ligand fields are known to stabilize the HS configuration and consequently they lead to low transition temperatures. Conversely, strong ligand fields stabilizes the LS configuration and drive to higher $T_{1/2}$.[9] Nevertheless, both parameters, cooperativity and $T_{1/2}$, have a certain degree of interdependence since the crystal packing may induce subtle electronic (electron donating or withdrawing) and / or steric (molecular distortion, chemical pressure) effects transmitted through the intermolecular contacts. Thus, the control and understanding of both parameters is a key issue in the SCO research area.

Polymorphism displayed by some SCO Fe^{II} complexes (especially discrete 0D systems) offers the possibility of evaluating how the intermolecular interactions influence both key parameters and constitutes a singular platform to shed light on the microscopic mechanisms that control the SCO phenomenon in the solid sate.[10] Most reported examples in SCO materials on polymorphism are related to the ways in which the complexes (including anions and solvents) can be packed in the crystal. In this respect, neutral complexes of the type $[Fe(L)_2(NCX)_2]$ (L = bidentate α-diimine ligand; X = S, Se) have afforded relevant examples of polymorphism. As far as we are aware, the first example of polymorphism structurally characterized corresponds to the complex *cis*-$[Fe(bt)_2(NCS)_2]$ (bt = 2,2'-bithiazoline) that crystallizes in two different polymorphs (A and B).[11] They display distinct crystal packing dominated by strong intermolecular S···S contacts, which drastically influence the geometry of the Fe^{II} coordination core. Polymorph A's coordination core exhibiting smaller angular distortion Θ and Σ parameters[12] ($\Sigma_{HS} = 78.75°$, $\Theta_{HS} = 230.4°$) undergoes a strong cooperative SCO centered at 181.5 K with a hysteresis 11.5 K wide, while the much more distorted Fe^{II} coordination geometry ($\Sigma_{HS} = 85.42°$, $\Theta_{HS} = 352.8°$) of polymorph B stabilizes the HS state at all temperatures even at pressures as high as 1 GPa.[11b] Similarly, the complex *trans*-$[Fe(abpt)_2(NCX)_2]$ (X=S, and Se; abpt = 4-amino-3,5-bis(pyridin-2-yl)-1,2,4-triazole) affords two polymorphs (A and B).[13] In the polymorphs A (X = S, Se) the abpt ligands, characterized by an intramolecular hydrogen bond between the amino group and the uncoordinated pyridine ring, are almost planar thus favoring a one-dimensional supramolecular

array of Fe^{II} complexes held together through π-π interactions. In contrast, the $NH_2\cdots$N(pyridyl) hydrogen bond vanishes in the polymorphs B allowing the uncoordinated pyridyl group to deviate 34° from planarity thereby generating a distinct two-dimensional network of π-π interactions.[13b] Polymorphs A display a gradual SCO behavior with $T_{1/2}$ = 180 K (X = S) and 224 K (X = Se), whereas polymorphs B are paramagnetic at all temperatures. Although the molecular distortions presented by both polymorphs are comparable, the polymorphs B display partial disruption of the π-delocalization in the abpt ligand and slightly longer Fe-N bond lengths. These subtle differences seem to be the reason of the different magnetic behavior. Indeed, the S-derivative of polymorph B displays a SCO at 0.86 GPa similar to that of the homologous derivative of polymorph A at ambient pressure.[13c]

In the same line, the complex *cis*-$[Fe(PMBiA)_2(NCS)_2]$ can be obtained in two different forms so-called polymorphs I and II.[14] Even if both complexes are thermally-induced spin crossover active they present quite different SCO curve features. Indeed, while polymorph I displays a very abrupt spin crossover curve with a hysteresis 5 K wide centered at 167 K, the SCO behavior of polymorph II is gradual with $T_{1/2}$ = 205 K. These two different behaviors have been explained by subtle differences in some angles of the Fe^{II} coordination core, and different S···HC intermolecular contacts established between adjacent complexes. Both parameters were demonstrated to be related to the abruptness of the spin transition curve, and therefore to the cooperativity of the SCO compound.

Another reported example of SCO polymorphs is the compound *fac*-$[Fe(dppa)_2(NCS)_2]$ (dppa is the tetradentate ligand (3-aminopropyl)bis(2-pyridylmethyl)amine). This compound crystallizes affording three different polymorphs (A-C). The magnetic susceptibility measurements revealed that while polymorph A and B exhibit SCO at 176 K (gradual without hysteresis) and 116 K (abrupt with hysteresis 8 K wide), respectively, polymorph C is paramagnetic at all temperatures. These differences in SCO behavior seem to be related to small differences detected in the Fe^{II} octahedral environment and to the quite distinct packing modes displayed by each compound.[15]

A more recent study of polymorphism and SCO relationships reported the compound *trans*-$[FeL^{Me}(NCS)_2]$ where L^{Me} is the tetradentate ligand *N,N'*-bis[(1-methyl-1,2,3-triazol-4-yl)methylene]propane-1,3diamine.[16] This compound crystallizes in two different monoclinic space groups C2/*c* (polymorph A) and $P2_1/n$ (polymorph B). Even if the structure of both polymorphs are very similar regarding the environment of the Fe^{II} ion, their crystal packing are

quite different establishing a larger number of hydrogen bonds (S···HC) for polymorph B than for polymorph A. These additional bonds are responsible for the stabilization of the LS state in polymorph B and, therefore, its almost 100 K higher transition temperature.

Additionally to the polymorphism, another approach to evaluate the effect of structural features on the modification of the SCO essential parameters is the comparison of isostructural compounds (*i.e*. chemically different compounds sharing the same structure). A relevant example is represented by the family of Fe^{II} mononuclear compounds [$Fe(R_2bapbpy)(NCX)_2$] (bapbpy = N6,N6'-di(pyridin-2-yl)-2,2'-bipyridine-6,6'-diamine, X= S or Se).[17] In general, and as demonstrated in previous works,[18] the substitution of S by Se on the NCX^- ligand leads to less cooperative SCO with higher transition temperatures because of the higher electronegativity of the former. This is, in general, the case for the [$Fe(R_2bapbpy)(NCX)_2$] series with the exception of complex [$Fe(R_2bapbpy)(NCX)_2$] where the Se derivate is more cooperative. The lack of single crystal X-ray data hindered an explanation for this observation but the authors hypothesized that structural factors could be behind this result.

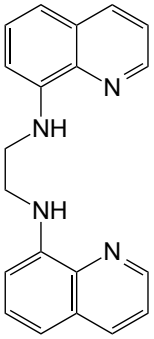

Scheme 1. Geometrical representation of the ligand bqen.

Here we report on an unprecedented example of polymorphism relating the racemic and homochiral forms of two Fe^{II} SCO complexes. More precisely, we present the synthesis and characterization of a new family of SCO mononuclear Fe^{II} complexes of general formula *cis*-[$Fe(bqen)(NCX)_2$] being bqen the tetradentate ligand *N*,*N*'-Bis(8-quinolyl)ethane-1,2-diamine (Scheme 1), and X=S or Se. Both thio- and selenocyanate derivatives afford two polymorphs that crystallize in the heterochiral orthorhombic *Pbca* space group (polymorph I) and in the homochiral trigonal $P3_121$ (or $P3_221$) space group (polymorph II). Each polymorph is accessible as a pure phase by the control of the synthetic method. We also intend to correlate the different SCO

temperatures and cooperativity degrees observed for each compound with the differences of the available crystal structures.

RESUL AND DISCUSIONS

Synthesis

The bqen ligand was synthesized according to the method reported in the literature.[19] The addition of a methanolic/ethanolic solution of bqen to a methanolic solution containing 1 equivalent of $Fe(SO_4)\cdot 7H_2O$ and 2 equivalents of KSCN (or KSeCN) led to the precipitation of a red solid labeled as **1** (**2**). It is worth noting the good reproducibility of this synthesis as the same products presenting the same structural and magnetic properties were obtained on repeated occasions. Powder X-ray diffraction (PXRD) patterns were also collected for **1** and **2** confirming their isostructurality (vide infra). Aiming at correlating the SCO behavior of **1** and **2** with their structure, numerous attempts for obtaining single crystals of these systems were carried out. However, the majority of the liquid-to-liquid diffusion strategies tried for this purpose were unsuccessful likely due to the oxidation of Fe^{II} triggered by the basic character of ligand bqen. This brought to the formation of brown (almost black) solutions that yielded poor crystalline solids of the same color. In view of these difficulties, two different approaches were followed: i) *Substitution of Fe^{II} ion with Ni^{II}*. The goal was to obtain the crystal structure of the non SCO-active analogous compounds *cis*-$[Ni(bqen)(NCX)_2]$ and, thus, to infer useful structural information for the homologous Fe^{II} complexes. Unexpectedly, following this strategy, square- and hexagonal-shaped single crystals were formed for both S and Se derivatives (Figures 1 left and middle). The four compounds show the same general formula $[Ni(bqen)(NCX)_2]$. The square-shaped thin plates X = S (**3**) and X = Se (**4**) turned out to be isostructural to **1** and **2**, as confirmed from comparison of the simulated single crystal X-ray patterns for **3** and **4** with the experimental PXRD patterns for **1** and **2**. The hexagonal-shaped crystals labeled **3'** (X = S) and **4'** (X = Se) exhibit different crystal structure, thereby revealing the existence of two polymorphs hereafter called polymorph I (compounds **1**, **2**, **3** and **4**) and polymorph II (compounds **3'** and **4'**).

ii) *Minimization of the contact time of Fe^{II} with bqen before the formation of the complex*. For this purpose an aqueous solution of the Fe^{II} salt was poured at the bottom of a test tube and a mixture of the KCNX salt and L in acetone was layered on the top. In order to slow down the

mixture of the reactants, both solutions were separated by an intermediate acetone/water (1:1) layer. In these conditions, a pure phase formed by hexagonal single crystals (see Figure 1 right) suitable for single crystal X-ray studies were obtained in a quantitative manner for the S and Se derivatives (compounds **1'** and **2'**, respectively). The crystal analysis for **1'** and **2'** (Fe^{II} derivatives) indicated that they are isostructural to **3'** and **4'** (Ni^{II} derivatives) and, therefore, they belong to polymorph II. Table 1 gathers a summary of all compounds obtained in this work.

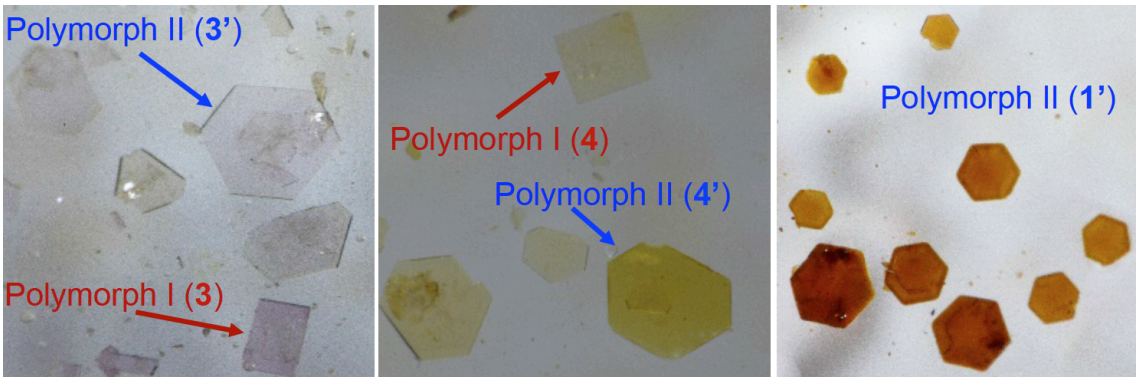

Figure 1. Optical images of the single crystals studied in this work: Mixtures of polymorphs I and II for [Ni(bqen)$(NCX)_2$] with X = S (**3** and **3'**) (left), and Se (**4** and **4'**) (middle). Pure phase of [Fe(bqen)$(NCS)_2$] polymorph II (**1'**) (right). The corresponding [Fe(bqen)$(NCSe)_2$] polymorph II (**2'**) is morphologically identical to **1'**.

Table 1. Summary of compounds presented in this work.

Compound	M^{II}	X	Texture	Polymorph
1	Fe	S	powder	I-orthorhombic
2	Fe	Se	powder	I-orthorhombic
3	Ni	S	crystals	I-orthorhombic
4	Ni	Se	crystals	I-orthorhombic
1'	Fe	S	crystals	II-trigonal
2'	Fe	Se	crystals	II-trigonal
3'	Ni	S	crystals	II-trigonal
4'	Ni	Se	crystals	II-trigonal

Aiming at understanding the origin of the formation of these polymorphs, the precipitation reaction of each of them was performed in different mixtures of solvents. Indeed, as explained before, in the case of Fe^{II} complexes, the use of methanol/ethanol solutions led invariably to the formation of polymorph I (**1** and **2**). Conversely, slow diffusion of acetone/water solutions led to hexagonal single crystals identified as polymorph II (**1'** and **2'**). In view of these results, numerous attempts to crystallize the polymorph I of the Fe^{II} compound were carried out in ethanol/methanol medium. Unfortunately, we did not succeed likely due to the low solubility of the bqen ligand in these solvents. Besides, the use of other solvents as CH_2Cl_2 or water in combination with alcohols systematically led to single crystals of polymorph II.

In the case of Ni^{II} derivatives, no clear correlation was observed between the obtained polymorph and the used solvents (see experimental section). Indeed, a mixture of both polymorphs was the most frequent result for this metal regardless of the used mixture of solvents.

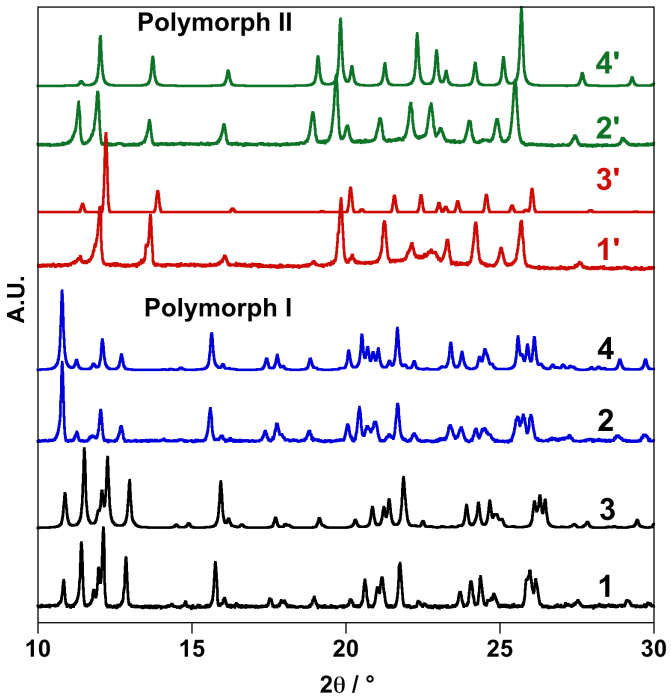

Figure 2. X-ray powder diffraction patterns. Polymorph I: **1** and **3** (X = S; black), **2** and **4** (X = Se; blue). Polymorph II: **1'** and **3'** (X = S; red), **2'** and **4'** (X = Se; green). Patterns for **3**, **4**, **3'** and **4'** were simulated from single crystal data.

X-ray powder diffraction

X-ray powder diffraction (XRPD) patterns for **1** and **2** (polymorph I) and **1'** and **2'** (polymorph II) are depicted in Figure 2. Moreover, the calculated patterns for Ni^{II} derivative complexes **3** and **4** (polymorph I) and **3'** and **4'** (polymorph II), obtained from single crystal diffraction (SCXR) (vide infra), are also showed for comparison. The similarity between the experimental X-ray patterns for compounds **1'** and **2'** (Figure 2) confirms their isostructurallity (polymorph II) whereas the comparison with their corresponding simulated spectra (Figure S1) indicates the presence of a pure phase. On the other hand, the comparison of the diffraction patterns of **1'** and **2'** with those of **1** and **2** clearly reveals that they correspond to different phases, whereas the latter correspond to isostructural phases (polymorph I). The simulated powder patterns of crystals **3** and **4** and **3'** and **4'** fit, as expected, the experimental powder patterns of **1** and **2** (powder compounds) and **1'** and **2'** (crystal compounds) confirming that they can be ascribed to polymorph I and polymorph II, respectively.

Spin crossover behavior

Magnetic properties. The thermal dependence of the $\chi_M T$ product (where χ_M is the molar magnetic susceptibility and T is the temperature) was measured for the four Fe^{II} compounds. The temperature scan rate was kept at 2 K min^{-1} for **2**, **1'** and **2'** while it was reduced at 1 K min^{-1} for **1** in order to minimize possible kinetic effects. The results are depicted in Figure 3. At 250 K, compounds **1** and **1'** display a $\chi_M T$ value of 3.50 and 3.33 cm^3 K mol^{-1}, respectively, in agreement with a Fe^{II} ion in the HS state. For **1**, this value remains constant down to 150 K. At lower temperatures $\chi_M T$ decreases, first gradually and then abruptly reaching a value of 0.5 cm^3 K mol^{-1} at 50 K ($T_{1/2}\downarrow$ = 86 K). This result clearly indicates an almost complete HS-to-LS transition of the Fe^{II} ions. The subsequent heating shows the reversibility of this process, characterized by an asymmetric hysteresis loop ($T_{1/2}\uparrow$ = 98 K). The asymmetric shape of the hysteresis and the low temperatures of the SCO suggest the occurrence of slow kinetics. In contrast, the polymorph **1'** presents a reversible abrupt SCO at higher temperatures ($T_{1/2}\downarrow$ = 142 K and $T_{1/2}\uparrow$ = 147) with a narrower hysteresis loop 5 K wide.

At 350 K, the $\chi_M T$ values of complexes **2** and **2'**, 3.53 and 3.36 cm^3 K mol^{-1}, respectively, are consistent with the almost fully populated HS state Fe^{II} ion. Upon cooling, $\chi_M T$ decreases gradually for both polymorphs reaching values of 0.34 and 0.28 cm^3 K mol^{-1} at

100 K. The almost complete SCO behaviors are characterized by $T_{1/2}$ centered at ca. 204 and 235 K for compounds **2** and **2'**, respectively. Despite the gradual nature of the SCO, **2'** displays a narrow hysteresis loop 5 K wide.

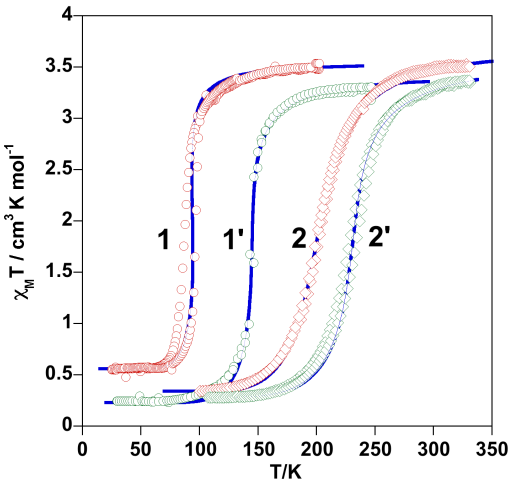

Figure 3. Magnetic behavior of compounds **1**, **1'**, **2** and **2'**.

Calorimetric properties. Differential scanning calorimetry (DSC) measurements were carried out for **1'**, **2** and **2'** in the cooling and heating modes. The corresponding anomalous variation of the heat capacity ΔC_p vs T plots is depicted in Figure 4. Compound **1** could not be measured since $T_{1/2}$ falls below the minimum temperature reached by our DSC device. The transition temperatures in the cooling ($T_{1/2}\downarrow$) and heating modes ($T_{1/2}\uparrow$) extracted from the maximum value of the ΔC_p vs T plots are $T_{1/2}\downarrow$ = 145 K and $T_{1/2}\uparrow$ = 146 K for **1'**, $T_{1/2}\downarrow$ = 197 K and $T_{1/2}\uparrow$ = 200 K for **2** and $T_{1/2}\downarrow$ = 232 K and $T_{1/2}\uparrow$ = 233 K for **2'**. These values fit satisfactorily with those obtained from the magnetic data. The average variation of enthalpy (ΔH) and entropy (ΔS) variations associated with the SCO calculated from the recorded DSC curves are 3.6 kJ mol^{-1} and 25.0 J mol^{-1} K^{-1} for **1'**, 8.5 kJ mol^{-1} and 43.1 J mol^{-1} K^{-1} for **2**, and 6.0 kJ mol^{-1} and 25.8 J mol^{-1} K^{-1} for **2'**. As expected, ΔS is larger than calculated from the purely electronic spin contribution (ΔS = 13.38 J K^{-1} mol^{-1}) for the LS $\leftrightarrow$ HS transition. The remaining excess corresponds to the entropic contributions stemming from the molecular vibrational modes and lattice phonons. Although, these ΔS values obtained are below those expected for a complete SCO in an

Fe^{II} complex (50-65 J mol^{-1} K^{-1}) they are in line with those reported for related compounds.[9b,18] This observation could be rationalized in terms of possible structural constraints induced by this type of rigid tetradentate ligand, which in turn could favor certain degree of incompleteness of the SCO, particularly in the HS state. Indeed, an unexpected relatively small increase of the Fe-N average bond length upon spin transition is observed (vide infra). These results strongly contrast with those observed for the aforementioned polymorphs A and B of the complex $[Fe(L^{Me})(NCS)_2]$ characterized by ΔS values of about 60 J K^{-1} mol^{-1}. The much larger ΔS values in the latter case may be related to the more flexible nature of the tetradentate ligand L^{Me}.[16]

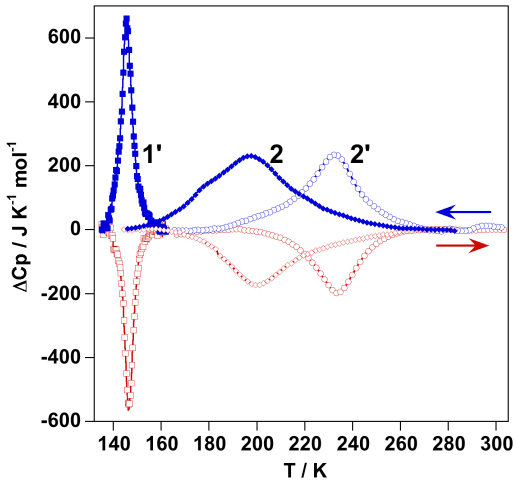

Figure 4. DSC measurements for the SCO compounds **1'**, **2** and **2'**.

Taking advantage of the obtained thermodynamic data, the spin conversions have been simulated and additional thermodynamic parameters have been inferred from eqn (1) derived from the regular solution model:[20]

$$ln\left[\frac{1-\gamma_{HS}}{\gamma_{HS}-\gamma_{HS}^{R}}\right] = \frac{\Delta H + \Gamma\,(1+\gamma_{HS}^{R}-2\gamma_{HS})}{RT} - \frac{\Delta S}{R} \qquad (1)$$

where ΔH, ΔS and Γ are the enthalpy and the entropy variations and the parameter accounting for the cooperative nature of the spin conversion, respectively. The molar HS fraction, γ_{HS}, has been deduced from the magnetic susceptibility through eqn (2):

$$\gamma_{HS} = [(\chi_M T) - (\chi_M T)_{LS}]/[(\chi_M T)_{HS} - (\chi_M T)_{LS}] \qquad (2)$$

The molar fraction $(\gamma_{HS})^R$ accounts for the HS species blocked at low temperatures and is calculated as follows (eqn (3)):

$$(\gamma_{HS})^R = (\chi_M T)^R / (\chi_M T)^{HS} \qquad (3)$$

$(\chi_M T)$ is the value of $\chi_M T$ at any temperature, $(\chi_M T)_{HS}$ is the $\chi_M T$ value of the pure HS state ($T \rightarrow \infty$), $(\chi_M T)_{LS} \approx 0$ is the $\chi_M T$ value of the pure LS and $(\chi_M T)^R$ represents the residual $\chi_M T$ value due to HS species blocked at low temperature. Given that ΔH, ΔS, $T_{1/2}$ and $(\chi_M T)^R$ have been estimated directly from the magnetic and / or the DSC curves, the fitted parameters were Γ and $(\chi_M T)_{HS}$. The obtained parameters for the best simulations together with the experimental values are gathered in Table 2.

Table 2. Thermodynamic parameters (see text).

Compound	**1**	**1'**	**2**	**2'**
ΔH / J mol^{-1}	4512	3628	8792	6063
ΔS / J K^{-1} mol^{-1}	48	25	43.1	25.8
Γ / J mol^{-1}	2000	2645	2473	3860
$T_{1/2}$	94	145	204	235
$C = \Gamma/2RT_{1/2}$	1.27	1.09	0.73	0.99
$\chi_M T$ / cm^3 K mol^{-1}	3.55	3.65	3.75	3.86
$(\gamma_{HS})^R$	0.16	0.06	0.09	0.07

Crystal structure of Polymorph I

Given that we did not succeed in synthesizing single crystals of compounds **1** and **2**, the analysis of the single crystal structures of the homologous isostructural Ni derivatives (compounds **3** and **4**) was undertaken. Tables S1 and S2 contain, respectively, a selection of relevant crystal data and Ni-N bond lengths and angles for **3** and **4**.

Ni(bqen)(NCS)$_2$ (3). The crystal structure of **3**, determined at 120 K, displays the orthorhombic *Pbca* space group. The asymmetric unit cell is formed by a Ni^{II} center surrounded by one tetradentate bqen ligand, which adopts a cis-α coordination mode, and two cis NCS

groups that complete the octahedral coordination sphere (see Figure 5a). The average Ni-N bond length, 2.086(6) Å, is characteristic of an octahedral Ni^{II} complex. The calculated angular octahedral distortion parameters are $\Sigma = 50.4(8)^\circ$ and $\Theta = 124(2)^\circ$.[12]

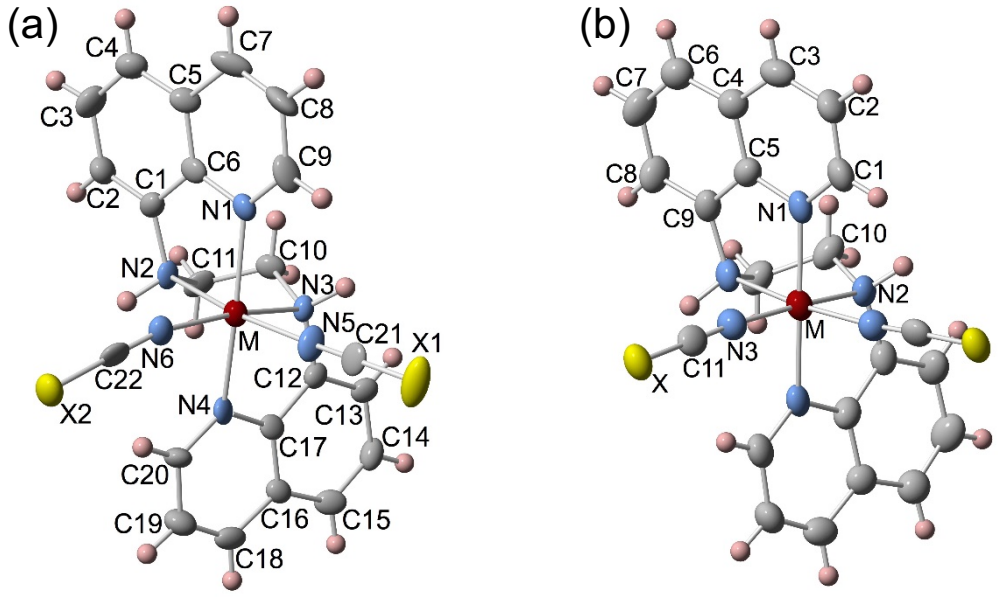

Figure 5. ORTEP representation of the coordination site for **3** and **4** (M = Ni, X = S, or Se) (polymorph I) (a) and for **1'**, **2'**, **3'** and **4'** (M = Fe or Ni; X = S or Se) (b). Thermal ellipsoids are represented at 50% probability.

The crystal packing is made up of neutral $[Ni(bqen)(NCSe)_2]$ molecules arranged in sheets defined by parallel rows of complexes, which extend along the [100] and stack along [010] directions. Within each row, the complexes display the same orientation and chirality, but the molecules of the adjacent rows are twisted approximately by an angle of 51° and display the opposite enantiomeric form (Figure 6a). Within the sheets, each complex interacts with its four closest neighbors via N-H···S hydrogen bonds, being the distances 3.244(6) Å between chains and 3.518(6) Å within chains. Moreover, six additional C-H···Se intermolecular contacts are observed between each complex and the six adjacent complexes. Two of these contacts (3.796(8) Å) are established with molecules within the chain and the remaining four with molecules situated in adjacent chains (3.639(7) and 3.712(8) Å). The racemic sheets are packed along the [001] direction through the interdigitation of the quinoline moieties that stack via π···π interactions (Figure 6b) as is evidenced by the numerous short C···C contacts, smaller than the sum of the C van der Waals radius, between adjacent aromatic rings (see Table S3 and Figure S2a).

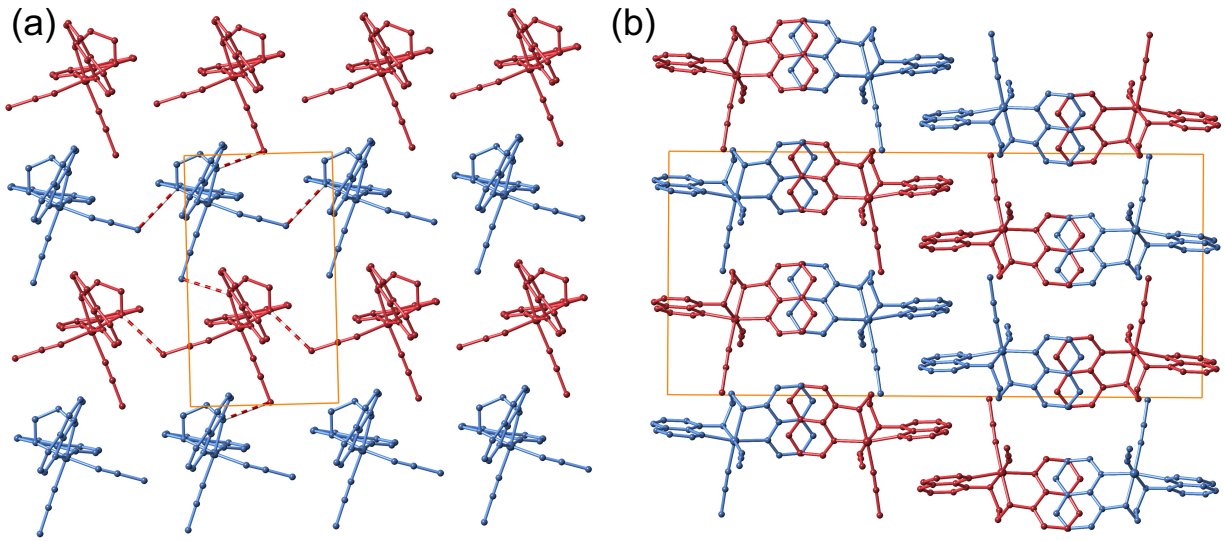

Figure 6. Compound **3** (polymorph I): (a) View of a fragment of sheet down to the [001] direction. (b) View of the packing of 4 consecutive sheets down to the [100] direction.

Ni(bqen)(NCSe)$_2$ (4). Structure of **4** was also determined at 120 K being its asymmetric unit cell analogous to that of **3**, presenting the same orthorhombic *Pbca* space group and similar crystal packing. However, the following relevant changes occur when moving from the S derivative (**3**) to the Se derivative (**4**): i) the average Ni-N bond length 2.091(5) Å and the octahedral distortion parameters (Σ = 52.2(6)° and Θ = 131(2)°) are slightly larger in relation to **3**; ii) the average distances of the NCX···N and NCX···HC interactions increaseby 0.10 and 0.05 Å, respectively; and iii) the average $\pi\cdots\pi$ short contacts between adjacent sheets are slightly larger for **4** (see Table S3 and Figure S2a).

Crystal structure of polymorph II

Tables S1 and S4 contain, respectively, a selection of relevant crystal data and Fe-N/Ni-N bond lengths and angles for **1'**, **2'**, **3'** and **4'**.

Fe(bqen)(NCS)$_2$ (1'). Hexagonal shaped single crystals of **1'** were measured at 120 (dark red) and 180 K (orange). At 120 K, the complex crystalizes in the trigonal chiral space group $P3_121$ (or $P3_221$ depending on the chirality of the complexes). The asymmetric unit includes half molecule of [Fe(bqen)(NCS)$_2$] generating an octahedral environment around the Fe^{II} center through a binary axis that bisects the angle defined by the two SCN$^-$ groups, the Fe^{II} ion and by the two amino groups (see Figure 5b). Thus, similarly to the Ni^{II} complexes **3** and **4**, the Fe^{II}

center is coordinated by the tetradentate ligand bqen, which adopts a cis-α coordination mode. The slightly distorted octahedral [$Fe^{II}N_6$] sphere (Σ_{LS} = 36(2)° and Θ_{LS} = 91(3)°) is completed with two equivalent negatively charged thiocyanate ligands in *cis* conformation. The average Fe-N bond length, 1.999(9) Å, is consistent with that of an Fe^{II} ion in LS configuration in good agreement with the magnetic data. The packing mode of **1'** is made up of sheets formed by complexes [Fe(bqen)$(NCS)_2$] which display the same orientation and, therefore, the same chirality (Figure 7a). Within the sheets, each complex interacts via N(2)H···S intermolecular interactions (3.342(7) Å) with four of its six adjacent neighbors (see Figure 7a). Furthermore, eight additional S···HC interactions take place between each complex and its six adjacent counterparts. Four of them (S···C(1)H = 3.569(12) Å) occur between the four closest neighbors whereas the remaining four interactions (S···C(8)H = 3.835(13) Å) are established with the two more distant neighbors.

Differently to **3** and **4**, the sheets are consecutively pillared in such a way that they are related by a ternary helical symmetry defining the infinite sequence ···, i, ii, iii, i,··· (Figure 7b) in which all the molecules present the same chirality, thereby giving enantiopure single crystals. Nevertheless, single crystals displaying either the $P3_121$ or $P3_221$ space group, differing in the chirality (Λ or Δ) complexes, were found within the same batch of crystals revealing that the compound is indeed a mixture of chiral crystals. Similarly to polymorphs I complex **1'** displays short C···C contacts indicating the occurrence of intermolecular π···π interactions between the quinoline moieties (see Table S5).

At 180 K the structure is basically the same as at 120 K, but the average Fe-N bond length is 0.171 Å longer. This change, although smaller than the 0.2 Å expected for $Fe^{II}N_6$ complexes, is consistent with the occurrence of a SCO from LS↔HS also evidenced by the color change of the crystal from dark red to orange. Besides, and as expected, the angular octahedral distortion parameters around the Fe^{II} center slightly increase with the LS↔HS spin state change ($\Delta\Sigma_{HL}$ = 37(2)° and $\Delta\Theta_{HL}$ = 73(3)°).

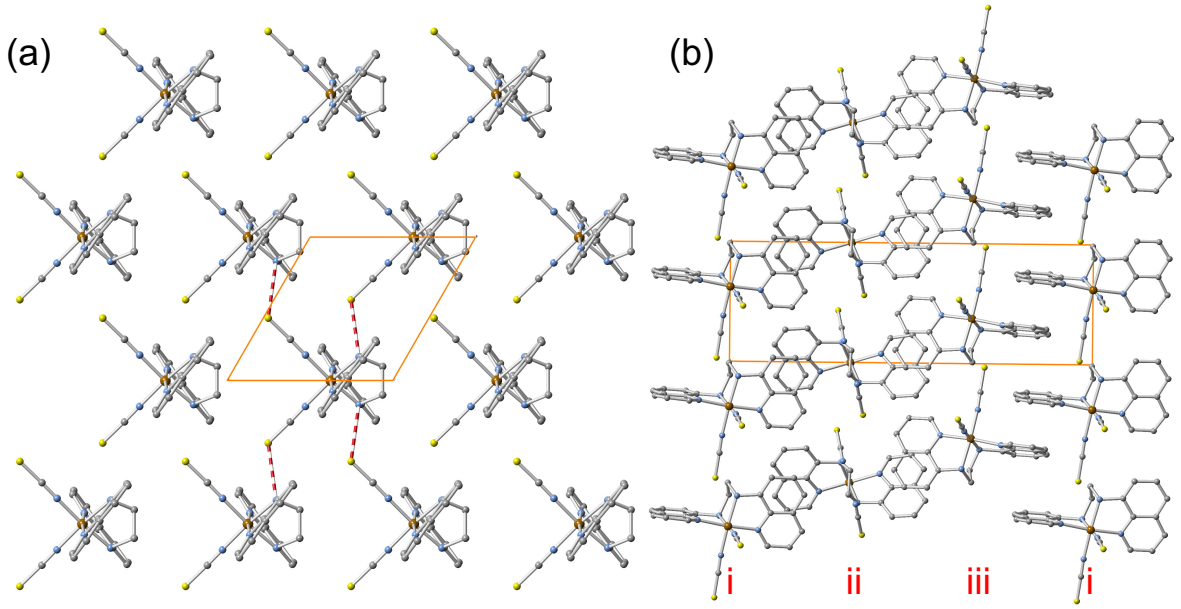

Figure 7. Compound **1'** (polymorph II). Perspective view down to [001] (a) and [100] (b) directions of a fragment of sheet and a stack of 4 consecutive sheets. In this case all the molecules display Λ configuration. Labels ···i, ii, iii, i··· indicate consecutive stacked chiral sheets related through a ternary helical axis running along [001]. Red dashed lines represent the NH···S interactions.

Fe(bqen)(NCSe)$_2$ (2'). Hexagonal shaped single crystals of **2'** were measured at 120 K (dark red) and 280 K (dark orange) resulting to be isostructural to **1'**. Indeed, at 120 K compound **2'** presents the same trigonal space group ($P3_121$) and a similar asymmetric unit to **1'**. At this temperature, the average Fe-N bond length equal to 1.989(12) Å is associated with the LS state of the Fe^{II} ion. The angular distortion from the regular octahedral geometry of the [Fe^{II}N$_6$] core gives the parameters Σ_{LS} = 36(2)° and Θ_{LS} = 102(6)°, which are clearly above those found for **1'**(LS). Likewise, the crystal packing observed for **2'** is essentially the same as that described for **1'**. However, it is worth noting that, likely due to the larger volume of Se compared to that of S, the arrangement of the mononuclear units, leads, in general, to longer intermolecular contacts. For example, the N(2)H···Se distances are 3.405(12) Å, namely 0.063 Å longer than for **1'**. Furthermore, the average CH···XCN intermolecular contact is practically the same to that of **1'** (3.694(13) vs 3.702(20) Å), while the π···π short contacts between the interdigitated quinoline moieties are slightly weaker in **2'** (Table S5).

At 280 K the structure of **2'** remains in the trigonal $P3_121$ space group. The increase of the unit cell volume ($\Delta V \approx 79$ Å^3) and the observed red to orange color change are accompanied by an increase of the average Fe-N bond length by 0.171 Å [2.160(14) Å] which suggests the

occurrence of an almost complete LS-to-HS transition of the Fe^{II} centers. Similarly to **1'**, the spin state change in **2'** also involves an increase of the angular distortion of the $[Fe^{II}N_6]$ octahedral geometry ($\Delta\Sigma_{HL}$ = 25(3)° and $\Delta\Theta_{HL}$ = 52(6)°).

Ni(bqen)(NCX)$_2$ (X = S(3'), Se(4')). The crystal structure of **3'** and **4'** have been measured at 120 K and as compounds **1'** and **2'**, display the trigonal space group $P3_121$. Both series of compounds are isostructural and consequently we refer to the structural description of **1'** and **2'**. Concerning the $[Ni^{II}N_6]$ coordination core, the average Ni-N bond length is 2.094(8) Å (X = S) and 2.086(9) Å (X = Se). These values are consistent with the ionic radius of Ni^{II} in an octahedral environment, which is approximately at half-way between the ionic radius of the HS and LS state of the Fe^{II} ion. Consistently, the $[Ni^{II}N_6]$ coordination site angular distortions are approximately in between values observed for the HS and LS states of the Fe^{II} in **1'** and **2'**, namely Σ = 50(2)° and Θ = 121(3)° (X = S) and Σ = 49(2)° and Θ = 128(4)° (X = Se) for **3'** and **4'**, respectively. The crystal packing of **3'** and **4'** shows short intermolecular contacts that are close to those observed for the homologous Fe^{II} compounds.

The replacement of S with Se provokes important modifications in the intermolecular contacts (see Table 3, Figure S2b). Let us highlight, for example, the increase of the NCX···HN distances by 0.087 Å.

Table 3. Average M-N bond lengths (Å), angular distortion parameters Θ and Σ (°) of the $[Fe^{II}N_6]$ coordination core and relevant average NCX···HY intermolecular contacts (Å) (X = S, Se; Y = N, C).

	Compound (M/X)		M-N	Θ(°)	Σ(°)	NCX···HN	NCX···HC
orthorhombic Polymorph I	**1** (Fe/S)						
	2 (Fe/Se)						
	3 (Ni/S)		2.086(6)	124(2)	50.4(8)	3.381(6)	3.716(8)
	4 (Ni/Se)		2.091(5)	131(2)	52.2(6)	3.482(5)	3.765(6)
Trigonal Polymorph II	**1'** (Fe/S)	LS	1.999(9)	91(3)	36(2)	3.342(7)	3.702(13)
		HS	2.170(6)	164(2)	73(1)	3.366(15)	3.678(17)
	2' (Fe/Se)	LS	1.989(12)	102(6)	36(2)	3.405(12)	3.694(20)
		HS	2.160(14)	154(6)	61(3)	3.389(12)	3.746(18)

	3' (Ni/S)	2.094(8)	121(3)	50(2)	3.336(11)	3.707(12)
	4' (Ni/Se)	2.086(9)	128(4)	49(2)	3.423(14)	3.712(17)

Discussion

The single crystal X-Ray diffraction study carried out during this work has revealed the presence of two different types of supramolecular arrangements of the mononuclear complexes $M(bqen)_2(NCX)_2$ (M = Fe or Ni, X = S or Se). The two different arrangements give rise to either the orthorhombic Pbca or the trigonal $P3_121$ (or $P3_221$) space group, which have been labeled as polymorph I and polymorph II, respectively.

By controlling certain synthetic parameters, a given polymorph can be obtained instead of the other. For example, the slow diffusion of a Fe^{II} (or Ni^{II}) salt solution and a solution of the qben ligand and the corresponding KXCN precursor in a water-acetone medium result in the exclusive formation of polymorph II. Similarly, the precipitation reaction using these precursors leads to a microcrystalline compound also assignable to polymorph II, as long as acetone and water are used as solvents. Contrarily, the same experiment performed in MeOH-EtOH solutions involves the formation of polymorph I.

This solvent-dependent effect, already observed on similar compounds,[13] does not seem to be the unique aspect determining the nature of the resulting polymorph. Indeed, the slow diffusion of the Ni^{II} salt on bqen and KXCN yielded mainly mixtures of both polymorphs regardless of the used solvents. All these observations suggest that the stability of both polymorphs is very close, as indicated by the similar intermolecular interactions established between complexes in the crystal and, indeed, only subtle differences in the preparation mode can discriminate one polymorph from the other.

Interestingly, the subtle differences in the structural features detected for each polymorph, essentially observed in their crystal packing, seems to be governed by the presence of either a racemic mixture (polymorph I) or a pure enantiomeric form (polymorph II) of the complexes within the structure. This observation makes the title compounds particularly interesting since the examples of synergy between chirality and SCO so far reported are relatively scarce in the literature.[21] Moreover, to the best of our knowledge, this is the first SCO polymorphic system where one of the polymorphs is chiral whereas the other represents a racemic mixture.

Besides, the slightly different arrangement of the complexes observed for each polymorph cause a remarkable impact on their SCO properties. To go deeper into the analysis of the magneto-structural correlations, we have analyzed, on one hand, the influence of the structural aspects on the SCO temperature ($T_{1/2}$) and an the other hand, the degree of cooperativity of the SCO:

i) SCO Temperature. The four SCO complexes display quite distinct $T_{1/2}$ transition temperatures: **1** (94 K), **1'** (145 K), **2** (204 K) and **2'** (235 K). At first glance, one can rapidly notice that the replacement of S with Se strongly influences $T_{1/2}$. Effectively, the difference in $T_{1/2}$ value between the seleno- and thiocyanate derivatives is about 100 K. These values are larger than those observed (40-75 K) for mononuclear $[Fe(L)_2(NCX)_2]$ complexes where L is an α-diimine ligand such as, for example, 1,10-phenanthroline,[22] 2,2'-bithiazoline[11,23] or 4-amino-3,5-bis(pyridin-2-yl)-1,2,4-triazole[13,], *N*-(2'-pyridylmethylene)-4-(phenylethynyl)aniline[24,25], but of the same order of magnitude than that observed for the system derived from the ligand L = 3-(2-pyridyl)-[1,2,3]triazolo[1,5-a]pyridine).[26,27] This effect may be associated with two main reasons. On one hand, the higher electronegativity of the S atom, comparing with that of Se, causes a larger electron density withdrawal from the N donor atom, thereby decreasing the ligand field around the Fe^{II} center and, consequently, stabilizing the HS form. On the other hand, the octahedral distortion around the Fe^{II} ion also influences $T_{1/2}$. Indeed, remarkable differences can be observed in the values of the angular distortion parameters (Θ and Σ) when comparing $SeCN^-$ and SCN^- counterparts. In general, the substitution of SCN^- by $SeCN^-$ leads to larger distortion parameters (see Table 3). However, we should not take into account the absolute values of these parameters but rather the differences between the HS and LS spin states [$\Delta\Theta_{HL}$ and $\Delta\Sigma_{HL}$]. Actually, it has been observed that the higher the $\Delta\Theta_{HL}$ and $\Delta\Sigma_{HL}$ values the lower the $T_{1/2}$.[8b] This is because higher $\Delta\Theta_{HL}$ and $\Delta\Sigma_{HL}$ values implies larger energy cost in terms of rearrangement of the ligands around the Fe^{II} ion upon the SCO and, consequently, it involves a stabilization of the HS form. Keeping this in mind, the [$\Delta\Theta_{HL}$; $\Delta\Sigma_{HL}$] values observed for **1'** [73(3)°; 37(2)°] are about 24% higher than for **2'** [52(6)°; 25(3)°] and, therefore, this extra octahedral distortion in **1'** may contribute to the observed large $T_{1/2}$ difference (90 K) between both compounds. Although the same comparison cannot be carried out between **1** and **2**, due to the lack of single crystals of these compounds, even larger differences in

[$\Delta\Theta_{HL}$; $\Delta\Sigma_{HL}$] values between SCN^- and $SeCN^-$ derivatives should be expected taking into account that the difference in $T_{1/2}$ is even higher (110 K).

In view of the lack of single crystal X-ray information for **1** and **2** (polymorph I), a direct correlation between [$\Delta\Theta_{HL}$; $\Delta\Sigma_{HL}$] and the difference in $T_{1/2}$ between the two different polymorphs **1** and **1'** (56 K) or **2** and **2'** (29 K) was not possible. However, the [Θ; Σ] values for the Ni^{II} derivatives: **3** [124(2); 50.4(8)], **3'** [121(3); 50(2)], **4** [131(2); 52.2(6)] and **4'** [128(4); 49(2)] are very similar, indicating that the influence of crystal packing on the angular distortion of the [$Ni^{II}N_6$] core is negligible. If we extrapolate this situation to the Fe^{II} title compounds, the differences in $T_{1/2}$ between the two polymorphs should be tentatively attributed to larger values of the [$\Delta\Theta_{HL}$; $\Delta\Sigma_{HL}$] parameters for polymorph I. It is worth noting that no significant differences in the average M^{II}-N bond lengths for M^{II} = Ni (**3**, **3'**, **4**, **4'**) and Fe (**1'**, **2'**) are observed and, consequently, this situation can also be extrapolated to **1** and **2** suggesting that the Fe-N bond lengths have a minor influence in $T_{1/2}$.

ii) Cooperativity. The measurements of the magnetic properties (Figure 3) of the cis-[Fe(bqen)$(NCX)_2$] complexes have revealed two well-differentiated types of SCO behaviors: a rather abrupt spin transition observed for compounds **1** and **1'** and a less abrupt conversion between the HS and the LS states registered for compounds **2** and **2'**. It seems, hence, that the selenocyanate ligand favors gradual spin transitions whereas the coordination of thiocyanate ligands leads to first order transitions. Indeed, the values of cooperativity calculated from simulations of the magnetic curves, defined as $C = \Gamma/2RT_{1/2}$, are 1.27 (**1**), 1.09 (**1'**), 0.73 (**2**), 0.99 (**2'**) (Table 2) and thereby consistent with these observations. Thus, aiming at establishing a correlation between the observed cooperativity and the structural aspects, we have analyzed the main parameters extracted from the available X-Ray data. More specifically, we have focused on the comparison between the Ni^{II} complex structures **3** (**3'**) (S derivatives) and **4** (**4'**) (Se derivatives) since they are isostructural to **1** (**1'**) and **2** (**2'**), respectively. The length of the intermolecular interaction NCX···HN seems to be behind the above explained observations as it present values of 3.381(3) (3.336(11)) Å and 3.482(5) (3.423(14)) Å for **3** (**3'**) and **4** (**4'**), respectively, and therefore a difference of ca. 0.1 Å. Besides, the $\pi\cdots\pi$ stacking

interactions are also stronger for the thiocyanate derivatives and may enhance the cooperativity of these complexes.

Compounds **2** and **2'** exhibit a subtle difference in cooperativity (C = 0.73 and 0.99, respectively), which may be originated by their different packing modes. Indeed, the slight differences observed on the NCX···HN (3.482(5) Å (**4**) and 3.423(14) Å (**4'**)) and NCX···HC distances (3.765(6) (**4**) and 3.712(17) (**4'**) Å) for their Ni^{II} counterparts supports this observation. However, this correlation is not observed for **1** and **1'**. Indeed, the former shows higher cooperativity (C = 1.27 vs 1.01) despite of the larger NCX···HN and NCX···HC intermolecular contacts observed for its counterpart **3**. This larger C value for **1** is most likely overestimated due to kinetic effects associated with the low $T_{1/2}$ (<100 K) values. This kinetics is responsible for the asymmetric appearance and width of the thermal hysteresis that overestimates the cooperativity parameter.

Conclusion

An unprecedented family of mononuclear complexes $[M^{II}(bqen)(NCX)_2]$ (M^{II} = Fe or Ni; X = S or Se) based on the tetradentate chelating ligand bqen has been synthesized and characterized. Single crystal X-ray studies have revealed that, depending on the synthetic procedure, these compounds (X = S and Se) crystallize in two different crystal systems leading to two types of polymorphs (I and II). While polymorph I crystallizes in the orthorhombic space group *Pbca*, polymorph II displays a trigonal $P3_121$ (or $P3_221$) space group differing mainly in their packing mode. Interestingly, the orthorhombic phase presents a racemic Λ-Δ mixture of chiral cis-$[M^{II}(bqen)(NCX)_2]$ complexes. In contrast, the trigonal phase is built of only one enantiomer. The four Fe^{II} derivatives undergo SCO behavior enabling, for the first time, to correlate the SCO properties with their racemic and chiral polymorphic forms. Although there are no sharp differences between the short intermolecular contacts of both polymorphs it is important to point out that the crystal packing generated by the chiral polymorphs, for X = S and Se, favors higher $T_{1/2}$ values than the corresponding racemic ones. Our results suggest that the differences in the crystal packing of each polymorph are subtly transferred to the $[Fe^{II}N_6]$ core and reflected on the change of the angular distortion parameters $\Delta\Sigma_{HL}$ and $\Delta\Theta_{HL}$ upon LS↔HS transition, which represents a different energy "cost" in terms of geometry change and hence a distinct $T_{1/2}$ value. This mechanism is, in part, responsible for the large change of $T_{1/2}$ when moving from the NCS^- to

the $NCSe^-$ derivatives in each polymorph, the other important influence being the electronic effects derived from the substitution of S with Se in NCX^- group. Finally, the small differences found in cooperativity for the four compounds can be explained taking into account the impact of the S ↔ Se replacement on the intermolecular interactions and the different crystal packing between the two polymorphs.

EXPERIMENTAL SECTION

Materials

N,*N*'-Bis(8-quinolyl)ethane-1,2-diamine (bqen). Ligand bqen was obtained using the same synthesis conditions published elsewhere.[19]

***Cis*-[Fe(bqen)(NCS)$_2$] (1, polymorph I)**. A solution of bqen (36.4 mg) in a hot mixture of MeOH and EtOH (14 mL and 10 mL) was added dropwise to a methanolic solution (8 mL) containing 22.4 mg of KSCN, 32.2 mg of $FeSO_4 \cdot 7H_2O$ and a catalytic amount of ascorbic acid (to avoid the Fe^{II} to Fe^{III} oxidation process). An instantaneous precipitation of a dark red solid was observed and the mixture was stirred for 30 additional minutes. Afterwards, the solid was filtered off, washed with methanol and dried under vacuum. Elemental analysis: calculated for $C_{22}H_{18}FeN_6S_2$: C, 54.33; N, 17.28; H, 3.73. Found: C, 53.84; N, 16.74; H, 3.70.

***Cis*-[Fe(bqen)(NCSe)$_2$] (2, polymorph I)**. A 9 mL methanol solution consisting of 24.8 mg of KSeCN, 24.0 mg of $FeSO_4 \cdot 7H_2O$ and a few milligrams of ascorbic acid (to avoid the Fe^{II} oxidation) was treated with a solution of 27.1 mg of bqen in 14 mL of hot ethanol. From almost the first drop a red precipitate was observed. The mixture was stirred for 30 additional minutes, the red solid was filtered off, washed with methanol and dried under vacuum. Elemental analysis: calculated for $C_{22}H_{18}FeN_6Se_2$: C, 45.54; N, 14.49; H, 3.13. Found: C, 44.59; N, 14.35; H, 3.01.

***Cis*-[Ni(bqen)(NCS)$_2$] (3, polymorph I)**. Crystals of **3** were obtained through liquid-to-liquid diffusion method using a 10 mL H-tube. One side of the tube was filled with a MeOH solution (2 mL) of $Ni(NO_3)_2$ (14.21 mg,) and KNCS (9.43 mg,) whereas, in the other side, a CH_2Cl_2 solution (0.5 mL) of 15.35 mg of bqen ligand was placed. The rest of the tube was filled with methanol and sealed. Two weeks after, a mixture of pale pink hexagonal-shaped crystals (**3**, polymorph I) and pale pink plate crystals (**3'**, polymorph II) were grown within the tube, collected and

separated with the aid of binocular lens. Since these crystals were used only as reference of polymorphs I and II, their composition was confirmed exclusively from crystallographic analysis.

***Cis*-[Ni(bqen)(NCSe)$_2$] (4, polymorph I)**. Crystals of **4** were prepared in a similar way as for **3**. In this case, one side of the tube was filled with a MeOH solution (2 mL) of $NiSO_4 \cdot 6H_2O$ (18.83 mg) and KNCSe (14.08 mg,). On the other side of the tube, a CH_2Cl_2 solution (2 mL) of 15.35 mg of bqen was placed. The rest of the tube was filled with methanol and sealed. After 3 weeks a pure phase made up of pale orange plate single crystals was formed. Similarly to **3** and **3'**, the composition of **4** was confirmed exclusively from crystallographic analysis.

***Cis*-[Fe(bqen)(NCS)$_2$] (1', polymorph II)**. Crystals of **1'** were obtained by diffusion methods using a layering tube where an aqueous solution (10 mL) of $Fe(ClO)_4$ (30 mg) was poured in the first place. Then, an interlayer acetone/water (1:1, 4 mL) was deposited on the previous aqueous phase and, finally, an acetone solution (10 mL) of bqen ligand (34.3 mg) and KSCN (14.9 mg) was layered on the top of the interlayer. One week later hexagonal orange crystals of **1'** were collected from the middle of the tube. Elemental analysis: calculated for $C_{22}H_{18}FeN_6S_2$: C, 54.33; N, 17.28; H, 3.73. Found: C, 53.89; N, 16.95; H, 3.77.

***Cis*-[Fe(bqen)(NCSe)$_2$] (2', polymorph II)**. Crystals of **2'** were prepared through an analogous strategy to the one used for obtaining **1'** but replacing KNCS with KSeCN (22.2 mg). Hexagonal orange crystals were observed in the middle part of the tube around one week after its preparation. Elemental analysis: calculated for $C_{22}H_{18}FeN_6Se_2$: C, 45.54; N, 14.49; H, 3.13. Found: C, 45.66; N, 14.85; H, 3.21.

***Cis*-[Ni(bqen)(NCS)$_2$] (3', polymorph II)**. Crystals of **3'** were obtained in the same batch as **3** (see above). They crystallize as hexagonal pale pink plates that represent the majority of the product. The composition of **3'** was confirmed exclusively from crystallographic analysis.

***Cis*-[Ni(bqen)(NCSe)$_2$] (4', polymorph II)**. Crystals of **4'** were obtained as a pure phase by diffusion methods using an H-shaped tube. In one side, a mixture of 11.62 mg of $NiCl_2 \cdot H_2O$ and 14.08 mg of KSCN in MeOH (1.5 mL) was added, while a solution of bqen ligand in CH_2Cl_2 (0.5 mL) was poured in the other side. The tube was finally filled with MeOH and sealed. Orange crystals of **4'** were collected four weeks later. The composition of **4'** was confirmed exclusively from crystallographic analysis

Physical measurements. Variable-temperature magnetic susceptibility data were recorded with a Quantum Design MPMS2 SQUID magnetometer equipped with a 7 T magnet, operating at 1 T and at temperatures 1.8-400 K. Experimental susceptibilities were corrected for diamagnetism of the constituent atoms by the use of Pascal's constants. Powder X-ray measurements where performed on a PANalytical Empyrean X-ray powder diffractometer (monochromatic Cu Kα radiation). Calorimetric measurements were performed using a differential scanning calorimeter Mettler Toledo DSC 821e. Low temperatures were obtained with an aluminium block attached to the sample holder, refrigerated with a flow of liquid nitrogen and stabilized at a temperature of 110 K. The sample holder was kept in a dry box under a flow of dry nitrogen gas to avoid water condensation. The measurements were carried out using around 10 mg of **1'**, **2'** (single crystals) or **2** (microcrystalline sample) sealed in aluminium pans with a mechanical crimp. Temperature and heat flow calibrations were made with standard samples of indium by using its melting transition (429.6 K, 28.45 J g^{-1}). An overall accuracy of ±0.2 K in temperature and ±2% in the heat capacity is estimated. The uncertainty increases for the determination of the anomalous enthalpy and entropy due to the subtraction of an unknown baseline.

Single crystal X-ray diffraction. Single-crystal X-ray data were collected on an Oxford Diffraction Supernova diffractometer using graphite mono-chromated MoKα radiation (λ = 0.71073 Å). A multi-scan absorption correction was performed. The structures were solved by direct methods using SHELXS-2014 and refined by full-matrix least squares on F^2 using SHELXL-2014.[28] Non-hydrogen atoms were refined anisotropically and hydrogen atoms were placed in calculated positions refined using idealized geometries (riding model) and assigned fixed isotropic displacement parameters.

Responses to the alerts type B appeared in some title compounds are provided in the corresponding CIF file and are related to low diffraction intensity of the crystals. Nevertheless, the crystallographic data fully convey all the chemical and structural meaning required to explain correctly the structures and the spin crossover behavior in this series of compounds. Supplementary crystallographic CIF data, [CCDC 1572177 (**1'**-HS), 1572178 (**1'**-LS), 1572179 (**2'**-HS), 1572180 (**2'**-LS), 1572181 (**3**), 1572182 (**4**), 1572183 (**3'**) and 1572184 (**4'**)], can be obtained free of charge from the Cambridge Crystallographic Data Centre.

ASSOCIATED CONTENT

(Word Style "TE_Supporting_Information"). **Supporting Information**. The supporting information (pages S1-S6) is available free of charge on the ACS Publications website at DOI: xxxxxxx.

Experimental and calculated XRPD patterns for **1'** and **2'** (Figure S1). Crystallographic parameters for **1'**, **2'**, **3**, **3'**, **4** and **4'** (Table S1). Selected bond lengths and angles for polymorph I (**3**, **4**) (Table S2). Intermolecular C···C contacts for polymorphs I and II of [Ni(bqen)(NCX)$_2$] (X = S, Se) (**3**, **3'**, **4** and **4'**) (Table S3). Selected bond lengths and angles for polymorph II (**1'**, **2'**, **3'**, **4'**) (Table S4). Crystal packing of polymorphs I and II for [Ni(bqen)(NCX)$_2$] (X = S, Se) (**3**, **3'**, **4** and **4'**) (Figure S2). Intermolecular C···C contacts for [Fe(bqen)(NCX)$_2$] (X = S, Se) polymorph II (Table S5).

AUTHOR INFORMATION

Corresponding Author

*Carlos.Bartual@uv.es

*jose.a.real@uv.es

ORCID

José Antonio Real: 0000-0002-2302-561X

Author Contributions

The manuscript was written through contributions of all authors. All authors have given approval to the final version of the manuscript.

Notes

The authors declare no competing financial interest.

ACKNOWLEDGMENT

We thank the Spanish Ministerio de Economía y Competitividad (MINECO) and FEDER funds (CTQ2013-46275-P and CTQ2016-78341-P and Unidad de Excelencia María de Maeztu MDM-2015-0538), Generalitat Valenciana (PROMETEO/2016/147) and EU Framework Program for Research and Innovation (RISE project number 734322). FJVM thanks MINECO for a predoctoral FPI grant.

REFERENCES

(1) (a) König, E. Nature and dynamics of the spin-state interconversion in metal-complexes. *Struct. Bonding (Berlin)* **1991**, *76*, 51-152; (b) Gütlich, P.; Hauser, A.; Spiering, H. Thermal and optical switching of iron(II) complexes. *Angew. Chem., Int. Ed. Engl.* **1994**, *33*, 2024-2054; (c) Real, J. A.; Gaspar, A. B.; Niel, V.; Muñoz, M. C. Communication between iron(II) building blocks in cooperative spin transition phenomena. *Coord. Chem. Rev.* **2003**, *236*, 121-141; (d) Gütlich, P.; Goodwin, H. A. Eds. Spin crossover in transition metal compounds I-III. *Top. Curr. Chem.* **2004**, Vols. *233-235*; (e) Real, J. A.; Gaspar, A. B.; Muñoz, M. C. Thermal, pressure and light switchable spin-crossover materials. *Dalton Trans.* **2005**, 2062-2079; (f) Bousseksou, A.; Molnár, G.; Salmon, L.; Nicolazzi, W. Molecular spin crossover phenomenon: recent achievements and prospects. *Chem. Soc. Rev.* **2011**, *40*, 3313-3335; (g) Halcrow, M. A. Ed. Spin-crossover materials: properties and applications. John Wiley & Sons. **2013**.

(2) Galet, A.; Gaspar, A. B.; Muñoz, M. C.; Bukin, G. V.; Levchenko, G.; Real, J. A. Tunable bistability in a three-dimensional spin-crossover sensory- and memory-functional material. *Adv. Mater.* **2005**, *17*, 2949-2953.

(3) Bousseksou, A.; Negre, N.; Goiran, M.; Salmon, L.; Tuchagues, J.-P.; Boillot, M.-L.; Boukheddaden, K.; Varret, F. Dynamic triggering of a spin-transition by a pulsed magnetic field. *Eur. Phys. J. B*, **2000**, *13*, 451-456.

(4) Decurtins, S.; Gütlich, P.; Hasselbach, K. M.; Hauser, A.; Spiering, H. Light-induced excited-spin-state trapping in iron(II) spin-crossover systems. Optical spectroscopic and magnetic susceptibility study. *Inorg. Chem.* **1985**, *24,* 2174-2178.

(5) (a) Ohba, M.; Yoneda, K.; Agustí, G.; Muñoz, M. C.; Gaspar, A. B.; Real, J. A.; Yamasaki, M.; Ando, H.; Nakao, Y.; Sakaki, S.; Kitagawa, S. Bidirectional chemo-switching of spin state in a microporous framework. *Angew. Chem. Int. Ed.* **2009**, *48*, 4767-4771; (b) Agustí, G.; Ohtani, R.; Yoneda, K.; Gaspar, A. B.; Ohba, M.; Sánchez-Royo, J. F.; Muñoz, M. C.; Kitagawa, S.; Real, J. A. Oxidative addition of halogens on open metal sites in a microporous spin-crossover coordination polymer. *Angew. Chem. Int. Ed.* **2009**, *48*, 8944-8947, (c) Southon, P. D.; Liu, L.; Fellows, E. A.; Price, D. J.; Halder, G. J.; Chapman, K. W.; Moubaraki, B.; Murray, K. S.; Letard, J.-F.; Kepert, C. J. Dynamics interplay between spin-crossover and host-guest function in a nanoporous metal-organic framework material. *J. Am. Chem. Soc.* **2009**, *131*, 10998-11009; (d) Arcís-Castillo, Z.; Muñoz-Lara F. J.; Muñoz, M. C.; Aravena, D.; Gaspar, A. B.; Sánchez-Royo, J. F.; Ruiz, E.; Ohba, M.; Matsuda, R.; Kitagawa, S.; Real, J. A. Reversible chemisorption of sulfur dioxide in a spin crossover porous coordination polymer. *Inorg. Chem.* **2013**, *52*, 12777-12783; (e) Muñoz, M. C.; Real, J. A. Thermo-, piezo-, photo- and chemo-switchable spin crossover iron(II)-metallocyanate based coordination polymers. *Coord. Chem. Rev.* **2011**, *255*, 2068-2093; (f) Ni, Z.-P.; Liu, J.-L.; Hoque, N.; Liu, W.; Li, J.-Y.; Chen, Y.-C.; Tong, M.-L. Recent advances in guest effects on spin-crossover behavior in Hofmann-type metal-organic frameworks. *Coord. Chem. Rev.* **2017**, *335*, 28-43.

(6). (a) Létard, J.-F.; Guionneau, P.; Goux-Capes, L. Towards spin crossover applications. *Top. Curr. Chem.* **2004**, *235*, 221-249; (b) Bousseksou, A.; Molnár, G.; Salmon, L.; Nicolazzi,.W. Molecular spin crossover phenomenon: Recent achievement and prospects. *Chem. Soc. Rev.* **2011**, *40*, 3313-3335; (c) Sato, O. Dynamic molecular crystals with switchable physical properties. *Nat. Chem.* **2016**, *8*, 644-656.

(7) (a) Gütlich, P.; Garcia, Y.; Goodwin, H. A. Spin crossover phenomena in Fe(II) complexes. *Chem. Soc. Rev.* **2000**, *29*, 419-427; (b) Gütlich, P.; Hauser, A.; Spiering, H. Thermal and optical switching of iron(II) complexes. *Angew. Chem. Int. Ed.* **1994**, *33*, 2024-2054.

(8) (a) Halcrow, M. A. Spin-crossover compounds with wide thermal hysteresis. *Chem. Lett.* **2014**, *43*, 1178-1188; (b) Halcrow, M. A. Structure: function relationships in molecular spin-crossover complexes. *Chem. Soc. Rev.*, **2011**, *40*, 4119-4142.

(9) (a) Luo, Y.-H.; Chen, L.; Wang, J.-W.; Wang, M.-X.; Zhang, Y.-W.; Sun, B.-W. Ligand field tuned spin crossover for an iron(II)-di(diamine) system. *Inorg. Chim. Acta* **2016**, *450*, 8-11; (b) Zheng, S.; Siegler, M. A.; Roubeau, O.; Bonnet, S. Influence of selenocyanate ligands on the

transition temperature and cooperativity of bapbpy-based Fe(II) spin-crossover compounds. *Inorg. Chem.* **2014**, *53*, 13162-13173.

(10) Tao, J.; Wei, R.-J.; Huang, R.-B.; Zheng, L.-S. Polymorphism in spin-crossover systems. *Chem. Soc. Rev.* **2012**, *41*, 703-737.

(11) (a) Ozarowski, A.; McGarvey, B. R.; Sarker, A. B.; Drake, J. E. EPR study of manganese(II) in two crystalline forms of bis(2,2'-bi-2-thiazoline)bis(thiocyanato)iron and the high-spin-low-spin transition that occurs in only one form. X-ray structure determination of both forms. *Inorg. Chem.* **1988**, *27*, 628-635; (b) Galet, A.; Gaspar, A. B.; Muñoz, M. C.; Levchenko, G.; Real, J. A. Pressure effect and crystal structure reinvestigations on the spin crossover system: $[Fe(bt)_2(NCS)_2]$ (bt = 2,2'-bithiazoline) polymorphs A and B. *Inorg. Chem.* **2006**, *45*, 9670-9679.

(12) Θ is defined as $\sum_{i=1}^{24}(60-\theta_i)$ being θ_i the angle generated by superposition of two opposite faces of the octahedron (there are four pairs of such superposition with six θ values each one). Σ represents octahedron distortion defined as the sum of deviations from 90º of the 12 *cis* N-Fe-N angles in the coordination sphere $\Sigma = \Sigma_{i=1}^{12}\left|\varphi_i - 90\right|$.

(13) (a) Moliner, N.; Muñoz, M. C.; van Koningsbruggen, P. J.; Real, J. A. Spin crossover in six-coordinate $[Fe(L)_2(NCX)_2]$ compounds with L = DPQ = 2,3-bis-(2'-pyridyl)-quinoxaline, ABPT = 4-amino-3,5-bis(pyridin-2-yl)-1,2,4-triazole and X=S, Se: synthesis, magnetic properties and single crystal studies. *Inorg. Chim. Acta* **1998**, *274*, 1-6; (b) Moliner, N.; Muñoz, M. C.; Létard, S.; Létard, J.-F.; Solans, X.; Burriel, R.; Castro, M.; Kahn, O.; Real, J. A. Spin-crossover in the $[Fe(abpt)_2(NCX)_2]$ (X=S, Se) system: structural, magnetic calorimetric and photomagnetic studies. *Inorg. Chim. Acta* **1999**, *291*, 279-288; (c) Gaspar, A. B.; Muñoz, M. C.; Moliner, N.; Ksenofontov, V.; Levchenko, G.; Gütlich, P.; Real, J. A. Polymorphism and pressure driven thermal spin crossover phenomenon in $[Fe(abpt)_2(NCX)_2]$ (X = S, Se): synthesis, structure and magnetic properties. *Monatsh. Chem.* **2003**, *134*, 285-294.

(14) (a) Marchivie, M.; Guionneau, P.; Létard, J.-F.; Chasseau, D. Towards direct correlations between spin-crossover and structural features in iron(II) complexes. *Acta Cryst.* **2003**, *B59*, 479-486; (b) Létard, J.-F.; Guionneau, P.; Rabardel, L.; Howard, J. A. K.; Goeta, A. E.; Chasseau, D.; Kahn, O. Structural, magnetic, and photomagnetic studies of a mononuclear iron(II) derivative exhibiting and exceptionally abrupt spin transition. Light-induced thermal hysteresis phenomenon. *Inorg. Chem.* **1998**, *37,* 4432-4441; (c) Létard, J.-F.; Montant, S.; Guionneau, P.;

Martin, P.; Le Calvez, A.; Freysz, E.; Chasseau, D.; Lapouyade, R.; Kahn, O. Large negative cubic hyperpolarizability for the spin-crossover compound cis-bis(thiocyanato)bis[N-(2-pyridylmethylene)aminobiphenyl]iron(II). *Chem. Commun.* **1997**, *8*, 745-746.

(15) Matouzenko, G. S.; Bousseksou, A.; Lecocq, S.; van Koningsbruggen, P. J.; Perrin, M.; Kahn O.; Collet, A. Polymorphism in spin transition systems. Crystal structure, magnetic properties, and Mössbauer spectroscopy of three polymorphic modifications of [Fe(DPPA)$(NCS)_2$] [DPPA (3-aminopropyl)bis(2-pyridylmethyl)amine]. *Inorg. Chem.* **1997**, *36*, 5869-5879.

(16) Hagiwara, H.; Okada, S. A polymorphism-dependent $T_{1/2}$ shift of 100 K in a hysteretic spin-crossover complex related to differences in intermolecular weak CH···X hydrogen bonds (X = S vs. S and N). *Chem. Commun.* **2016**, *52*, 815-818.

(17) (a) Bonnet, S.; Siegler, M. A.; Sanchez Costa, J.; Molnar, G.; Bousseksou, A.; Spek, A. L.; Gamez, P.; Reedijk, J. A two-step spin crossover mononuclear iron(II) complex with a [HS-LS-LS] intermediate phase. *Chem. Commun.* **2008**, 5619-5621; (b) Arcís-Castillo, Z.; Zheng, S.; Siegler, M. A.; Roubeau, O.; Bedoui, S.; Bonnet, S. Tuning the transition temperature and cooperativity of bapbpy-based mononuclear spin-crossover compounds: interplay between molecular and crystal engineering. *Chem. Eur. J.* **2011**, *17*, 14826-14836.

(18) Bréfuel, N.; Shova, S.; Lipkowski, J.; Tuchagues, J.-P. Fe^{II} bi-stable materials based on dissymmetrical ligands: N_4 Schiff bases including 2-pyridyl and 5-methylimidazol-4-yl ring. *Chem. Mater.* **2006**, *18,* 5467-5479.

(19) England, J.; Britovsek, G. J. P.; Rabadia, N.; White, A. J. P. Ligand topology variations and the importance of ligand field strength in non-heme iron catalized oxidations of alkanes. *Inorg. Chem.* **2007**, *46*, 3752-3767.

(20) (a) Slichter, C. P.; Drickamer, H. G. Pressure-induced electronic changes in compounds of iron. *J. Chem. Phys.* **1972**, *56*, 2142-2160; (b) Martin, J. P.; Zarembowitch, J.; Bousseksou, A.; Dworkin, A.; Haasnoot, J. G.; Varret, F. Solid state effects on spin transitions: magnetic, calorimetric, and Mössbauer-effect properties of $[Fe_xCo_{1-x}(4,4'\text{-bis-}1,2,4\text{-triazole})_2(NCS)_2]\cdot H_2O$ mixed-crystal compounds. *Inorg. Chem.* **1994**, *33*, 6325-6333; (c) Martin, J. P.; Zarembowitch, J.; Dworkin, A.; Haasnoot, J. G.; Codjovi, E. Solid-state effects in spin transitions: role of

iron(II) dilution in the magnetic and calorimetric properties of the series $[Fe_xNi_{1-x}(4,4'\text{-bis}(1,2,4\text{-triazole}))_2(NCS)_2]\cdot H_2O$. *Inorg. Chem.* **1994**, *33*, 2617-2623.

(21) (a) Sunatsuki, Y.; Ikuta, Y.; Matsumoto, N.; Ohta, H.; Kojima, M.; Iijima, S.; Hayami, S.; Maeda, Y.; Kaizaki, S.; Dahan, F.; Tuchagues, J. P. An unprecedented homochiral mixed-valence spin-crossover compound. *Angew. Chem., Int. Ed.* **2003**, *42*, 1614-1618; (b) Hashibe, T.; Fujinami, T.; Furusho, D.; Matsumoto, N.; Sunatsuki, Y. Chiral spin crossover iron(II) complex, fac-Λ-$[Fe^{II}(HLR)_3](ClO_4)_2$·EtOH (HLR = 2-methylimidazol-4-yl-methylideneamino-R-(+)-1-methylphenyl). *Inorg. Chim. Acta* **2011**, *375*, 338-342; (c) Sunatsuki, Y.; Miyahara, S.; Sasaki, Y.; Suzuki, T.; Kojimaa, M.; Matsumoto, N. Conglomerate crystallization, chiral recognition and spin-crossover in a host-guest complex consisting of Fe^{III} complexes (host) and $[Cr(ox)_3]^{3-}$ (guest). *CrystEngComm* **2012**, *14*, 6377-6380; (d) Ohkoshi, S.; Takano, S.; Imoto, K.; Yoshikiyo, M.; Namai A.; Tokoro, H. 90-degree optical switching of output second-harmonic light in chiral photomagnet. *Nat. Photonics* **2014**, *8*, 65-71; (e) Liu, W.; Bao, X.; Mao, L. L.; Tucek, J.; Zboril, R.; Liu, J. L.; Guo, F. S.; Ni, Z. P.; Tong, M. L. A chiral spin crossover metal-organic framework. *Chem. Commun.* **2014**, *50*, 4059-4061; (f) Romero-Morcillo, T.; Valverde-Muñoz, F. J.; Muñoz, M. C.; Herrera, J. M.; Colacio, E.; Real, J. A. Two-step spin crossover behaviour in the chiral one-dimensional coordination polymer $[Fe(HAT)(NCS)_2]_\infty$. *RSC Adv.* **2015**, *5*, 69782-69789; (g) Sekimoto, Y.; Karim, M. R.; Saigo, N.; Ohtani, R.; Nakamura, M.; Hayami, S. Crystal structures and spin-crossover behavior of iron(II) complexes with chiral and racemic ligands. *Eur. J. Inorg. Chem.* **2017**, 1049-1053.

(22) Sorai, M .; Seki, S.Phonon coupled cooperative low-spin $^1A_1$high-spin $^5T_2$ transition in $[Fe(phen)_2(NCS)_2]$ and $[Fe(phen)_2(NCSe)_2]$ crystals. *J. Phys Chem. Solids* **1974**, *35*, 555-570.

(23) König, E. Ritter, G.; Dengler, J.; Nelso, J. Detailed study of the quintet↔singlet spin transition in bis(selenocyanato)bis(2,2'-bithiazoline)iron(II). Inorg. Chem. 1989, 28, 611-.

(24) Létard, J. F.; Guionneau, P.; Codjovi, E.; Lavastre, O.; Bravic, G.; Chasseau, D.; Kahn, O. Wide Thermal Hysteresis for the Mononuclear Spin-Crossover Compound *cis*-Bis(thiocyanato)bis[*N*-(2'-pyridylmethylene)-4-(phenylethynyl)anilino]iron(II) *J. Am. Chem. Soc.*, 1997, **119**, 10861-10862.

(25) Tailleur, E.; Marchivie, M.; Daro, N.; Chastanet, G.; Guionneau, P. Thermal spin-crossover with a large hysteresis spanning room temperature in a mononuclear complex Chem. Commun **2017**, *53*, 4763-4766.

(26) Sheu, C.-F.; Chen, K.; Chen, S.-M.; Wen, Y.-S.; Lee,G.-H.; Chen,J.-M.; Lee, J.-F. Cheng, B. M.; Sheu, H. S.; Yasuda, N.; Ozawa, Y.; Toriumi, K.; Wang, Y. Structure and electronic configuration of an iron(II) complex in a LIESST state: a pump and probe method. *Chem. Eur. J.* **2009**, *15*, 2384-2393.

(27) Arcís-Castillo, Z.; Piñeiro-López, L.; Muñoz, M. C.; Ballesteros, R.; Abarca, B.; Real, J. A. Structural, magnetic and calorimetric studies of a crystalline phase of the spin crossover compound $[Fe(tzpy)_2(NCSe)_2]$. *CrystEngComm*, **2013**, *15*, 3455-3462.

(28) Sheldrick, G. M. SHELXL-2014, University of Göttingen, Germany, **2014**.

For Table of Contents Only

Chiral and racemic polymorphic forms of the [Fe(bqen)(NCX)$_2$] (X = Se, Se) complexes provide an unprecedented example on the relevant role of the crystal packing in spin crossover complexes.

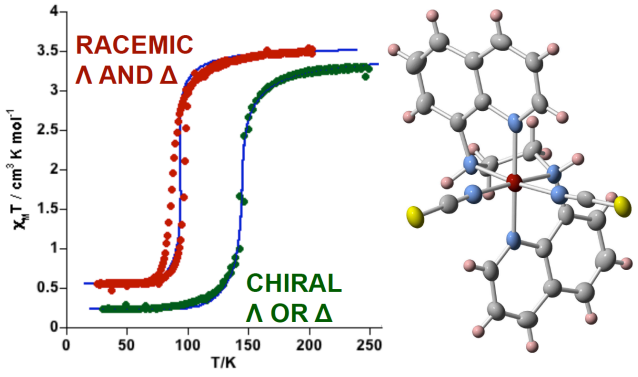

Supporting Information

Chiral and racemic spin crossover polymorphs in a family of mononuclear Iron(II) compounds

Carlos Bartual-Murgui,[a] Lucía Piñeiro-López,[a] F. Javier Valverde-Muñoz,[a] M. Carmen Muñoz,[b] Maksym Seredyuk,[a,c] José Antonio Real*[a]*

[a]Institut de Ciència Molecular (ICMol), Departament de Química Inorgànica Universitat de València C/ Catedrático José Beltrán Martínez, 2, 46980 Paterna (Valencia), Spain.

[b]Departamento de Física Aplicada Universitat Politècnica de València Camino de Vera s/n, 46022 Valencia, Spain.

[c]Taras Shevchenko National University, Department of Chemistry, Volodymyrska Str. 64, Kyiv 01601, Ukraine

*Carlos.Bartual@uv.es

*jose.a.real@uv.es

Figure S1. Experimental and calculated XRPD patterns for **1'** and **2'**.

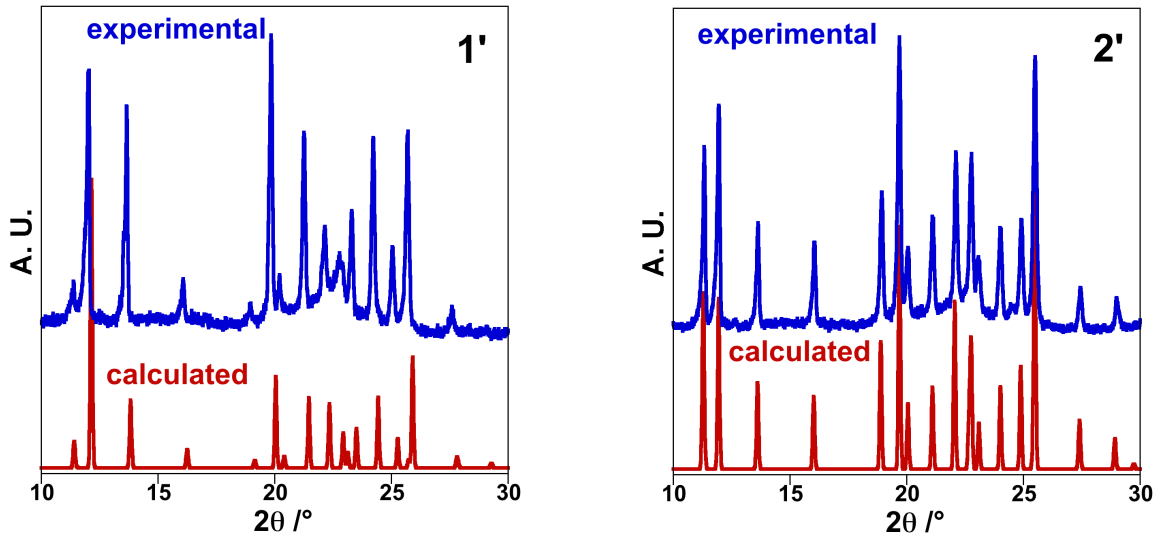

Table S1. Crystallographic parameters for **1'**, **2', 3**, **3'**, **4** and **4'**.

Compound	**1'**		**2'**		**3**	**3'**	**4**	**4'**
Temperature (K)	**120.0**	**180.0**	**120.0**	**280.0**	**120**	**120**	**120**	**120**
Empirical formula	$C_{22}H_{18}FeN_6S_2$		$C_{22}H_{18}FeN_6Se_2$		$C_{22}H_{18}NiN_6S_2$		$C_{22}H_{18}NiN_6Se_2$	
Mr	486.39		580.19		489.25		583.05	
Crystal system	trigonal		trigonal		orthorhombic	trigonal	orthorhombic	trigonal
Space group	$P3_121$		$P3_121$		*P*bca	$P3_221$	*P*bca	$P3_121$
Crystal size (mm)	0.10x0.10x0.05		0.11x0.065x0.007		0.08x0.07x 0.01	0.15x0.14x 0.02	0.12x0.11x 0.01	0.1x0.08x 0.01
a (Å)	8.7615(5)	8.851(5)	8.8671(4)	9.0083(9)	8.7159(3)	8.8021(3)	8.9128(3)	8.9459(4)
b (Å)	8.7615(5)	8.851(5)	8.8671(4)	9.0083(9)	14.7855(7)	8.8021(3)	14.8812(5)	8.9459(4)
c (Å)	22.9329(14)	23.244(5)	23.087(2)	23.5056(19)	32.4806(17)	23.1511(15)	32.614(2)	23.1874(14)
α (°)	90				90	90	90	90
β (°)								90
γ (°)	120					120		120
V (Å^3)	1524.6(2)	1577.0(18)	1572.0(2)	1651.9(4)	4185.7(3)	1553.37(15)	4325.7(3)	1607.05(17)
Z	3		3		8	3	8	3

Table S1 cont. Crystallographic parameters for **1'**, **2', 3**, **3'**, **4** and **4'**.

Compound	**1'**		**2'**		**3**	**3'**	**4**	**4'**
D_c (mg cm^{-3})	1.589	1.536	1.851	1.750	1.553	1.569	1.784	1.807
F(000)	750	750	864	858	2016	756	2288	864
μ (Mo-K_α)(mm^{-1})	0.971	0.939	4.219	4.012	1.150	1.162	4.285	0.994
No. of total reflections	2728	2767	2639	2738	4271	2107	5491	2181
No. of reflections [I>2 $\sigma(I)$]	1565	1688	1697	998	1762	1332	3462	1623
R [I>2 $\sigma(I)$][a]	0.0859	0.0735	0.0833	0.0852	0.0860	0.0790	0.0655	0.0706
R [all data][a]	0.1581	0.1347	0.1337	0.2344	0.2202	0.139	0.1198	0.1033
S	1.034	1.038	1.006	0.948	1.039	1.039	1.036	1.017

[a] $R = \Sigma \, ||F_o| - |F_c|| \, / \, \Sigma \, |F_o|$

Table S2. Selected Ni-N bond lengths (Å) and angles (°) for polymorph I (**3**, **4**).

	3	**4**
Ni1 N1	2.111(6)	2.105(5)
Ni1 N2	2.102(6)	2.103(5)
Ni1 N3	2.124(5)	2.123(5)
Ni1 N4	2.101(6)	2.108(5)
Ni1 N5	2.038(7)	2.054(5)
Ni1 N6	2.039(6)	2.056(5)
N1 Ni1 N3	92.7(2)	93.6(2)
N2 Ni1 N1	80.0(3)	79.7(2)
N2 Ni1 N3	84.3(2)	84.2(2)
N4 Ni1 N2	90.2(2)	90.9(2)
N4 Ni1 N3	80.2(2)	79.8(2)
N5 Ni1 N1	95.6(3)	95.7(2)
N5 Ni1 N3	91.2(2)	90.8(2)
N5 Ni1 N4	93.6(3)	93.1(2)
N5 Ni1 N6	92.3(2)	92.6(2)
N6 Ni1 N1	95.0(2)	94.4(2)
N6 Ni1 N2	92.8(2)	93.0(2)
N6 Ni1 N4	91.6(3)	91.7(2)

Table S3. Comparison between the C···C contacts (Å) of the trigonal and orthorhombic forms of the [Ni(bqen)$(NCX)_2$] series (X = S, Se). Only contacts shorter than the sum of the van der Waals radius of C (c.a. 3.7 Å) are considered.

[Ni(bqen)$(NCX)_2$]					
Trigonal			**Orthorhombic**		
	X = S (**3'**)	X = Se (**4'**)		X = S (**3**)	X = Se (**4**)
π-π contacts					
C1···C6	3.319(13)	3.430(20)	C13···C19	3.658(11)	
C1···C7	3.422(15)	3.430(20)	C14···C19	3.455(11)	3.443(8)
C2···C6	3.619(14)	3.653(22)	C15···C19	3.408(12)	3.405(8)
C2···C7	3.507(17)	3.506(22)	C16···C19	3.580(12)	3.642(9)
C2···C8	3.513(17)	3.517(18)	C15···C20	3.320(10)	3.381(9)
C2···C9	3.598(14)	3.653(22)	C14···C20	3.537(10)	3.589(8)
C3···C8	3.628(14)	3.639(17)	2x(C16···C14)	3.631 (10)	3.655(8)
C7···C7'	3.619(16)		C7···C1	3.593(11)	3.610(8)
2x(C7···C8)	3.685(16)		C7···C6	3.587(10)	3.676(8)
Other contacts					
C10···C6	3.682(13)	3.767(27)	C22···C7	3.236(12)	3.247(9)
C11···C2	3.634(16)	3.662(22)	C22···C8	3.613(12)	3.514(9)
			C21···C11	3.609(10)	3.695(8)
			C22···C11	3.659(10)	3.684(8)
			C11···C15	3.538(13)	3.509(9)

Table S4. Selected Fe-N/Ni-N bond lengths (Å) and angles (°) for polymorph II (**1'**, **2'**, **3'**, **4'**).

	1'-HS	**1'-LS**	**2'-HS**	**2'-LS**		**3'**	**4'**
Fe N1	2.192(5)	2.007(7)	2.178(11)	1.990(11)	Ni1 N1	2.098(7)	2.096(9)
Fe N2	2.228(6)	2.033(8)	2.218(14)	2.015(12)	Ni1 N2	2.117(8)	2.110(9)
Fe N3	2.085(7)	1.959(8)	2.086(16)	1.965(13)	Ni1 N3	2.068(9)	2.052(10)
N1 Fe N2	91.3(2)	92.6(3)	91.9(5)	82.9(5)	N1 Ni1 N2	80.6(3)	80.8(4)
N1 Fe N2	76.6(2)	83.3(3)	77.7(5)	93.0(4)	N1 Ni1 N2	92.5(3)	93.9(4)
N2 Fe N2	79.6(3)	85.5(4)	83.4(8)	85.9(7)	N2 Ni1 N2	83.8(5)	83.6(6)
N3 Fe N1	93.5(2)	92.3(3)	94.5(5)	93.5(5)	N3 Ni1 N1	93.2(3)	93.6(4)
N3 Fe N1	96.9(2)	91.5(3)	95.0(5)	90.5(4)	N3 Ni1 N1	93.2(3)	91.4(4)
N3 Fe N2	92.7(2)	90.9(3)	92.3(6)	91.9(5)	N3 Ni1 N2	91.9(3)	92.5(4)
N3 Fe N3	96.7(4)	93.0(5)	92.9(10)	90.5(8)	N3 Ni1 N3	93.1(5)	92.0(6)

Figure S2. Crystal packing of polymorphs I (orthorhombic, **3**, **4**) (a) and II (trigonal **3'**, **4'**) (b) of [Ni(bqen)(NCX)$_2$] displaying the C···C short contacts gathered in Table S3.

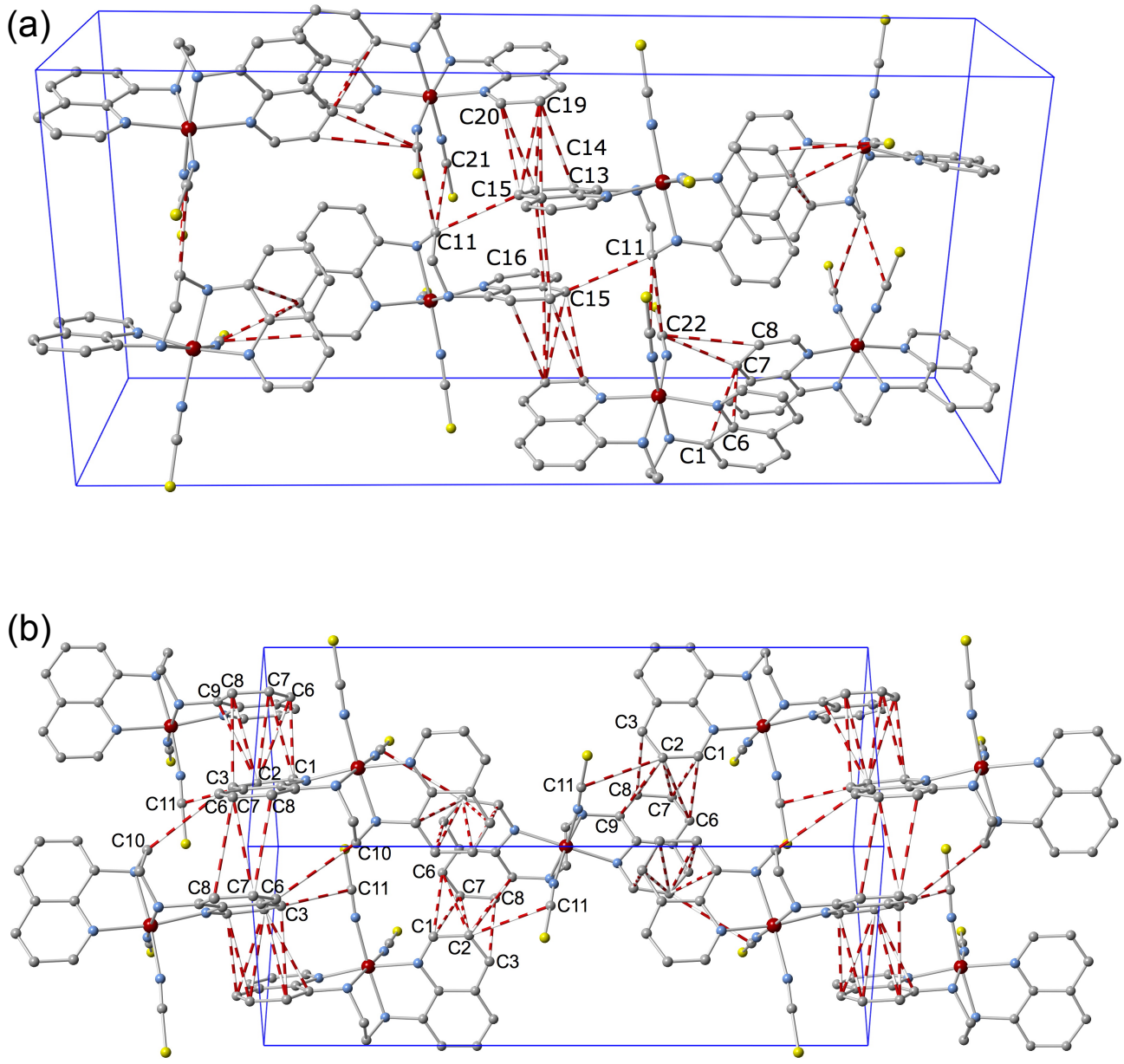

Table S5. Comparison between the C···C contacts (Å) of the trigonal polymorphs [Fe(bqen)$(NCX)_2$] series (X = S, Se) in the LS and HS spin states.. Only contacts shorter than the sum of the van der Waals radius of C (c.a. 3.7 Å) are considered.

	[Fe(bqen)$(NCX)_2$], Polymorph II (trigonal)			
	1' (X = S)		**2' (X = Se)**	
Spin State	**HS**	**LS**	**HS**	**LS**
π···π short contacts				
C1···C6	3.384(14)	3.341(12)	3.460(46)	3.383(18)
C1···C7	3.452(15)	3.454(15)	3.418(38)	3.468(21)
C2···C6		3.596(13)		3.586(19)
C2···C7	3.595(18)	3.499(16)	3.533(39)	3.465(23)
C2···C8	3.545(17)	3.535(16)	3.566(31)	3.538(23)
C2···C9		3.661(12)	3.689(31)	3.659(19)
C3···C8	3.692(15)	3.572(13)		3.636(19)
C7···C8	3.644(16)			
C7···C7	3.575(16)	3.626(22)		
Other C···C short contacts				
C6···C10	3.645(17)	3.600(15)		3.655(20)
C7···C11		3.679(16)		
C2···C11	3.677(15)	3.674(15)		